

Threshold of Singularity Formation in the Semilinear Wave Equation

Steven L. Liebling

Department of Physics, Long Island University – C.W. Post Campus, Brookville, NY 11548

(Dated: October 19, 2018)

Solutions of the semilinear wave equation are found numerically in three spatial dimensions with no assumed symmetry using distributed adaptive mesh refinement. The threshold of singularity formation is studied for the two cases in which the exponent of the nonlinear term is either $p = 5$ or $p = 7$. Near the threshold of singularity formation, numerical solutions suggest an approach to self-similarity for the $p = 7$ case and an approach to a scale evolving static solution for $p = 5$.

I. INTRODUCTION

One area of interest within the context of a nonlinear wave equation is the emergence of a singularity from smooth initial data. Among the issues raised by the formation of a singularity, the nature of the threshold for such formation is of particular interest. A number of past studies have addressed this threshold numerically in the nonlinear sigma model in both two [1, 2] and three [3, 4, 5, 6, 7] spatial dimensions. Here, I study the semilinear wave equation following the work of [8] which considers the formation of singularities in the model restricted to spherical symmetry.

A scalar field, ϕ , obeys the wave equation

$$\square\phi = \phi^p \quad (1)$$

for p odd (preserving the symmetry $\phi \rightarrow -\phi$). In three dimensions with Cartesian coordinates, this equation becomes

$$\ddot{\phi} = \phi_{,xx} + \phi_{,yy} + \phi_{,zz} + \phi^p, \quad (2)$$

where commas indicate partial derivatives with respect to subscripted coordinates and an overdot indicates partial differentiation with respect to time. Solutions are found numerically by rewriting the equation of motion (2) in first differential order form and replacing derivatives with second order accurate finite difference approximations. These finite difference equations are solved with an iterative Crank-Nicholson scheme. In order to achieve the dynamic range and resolution needed to resolve the features occurring on such small scales in this model, adaptive mesh refinement is used. In fact, the code necessary for this is achieved with minimal modification to the code used in [6, 7], and the reader is referred to these earlier papers for computational details. These changes consist of: (1) making the association $\phi \equiv \chi$, (2) replacing the nonlinear term in the evolution update of that model with the last term of Eq. (2), and (3) removing the regularity condition on the scalar field at the origin. As is common, an outgoing Robin boundary condition is applied at the outer boundaries assuming a spherical outgoing front. While not perfect, the outer boundary is generally far enough away from the central dynamics so that the boundary condition has no effect.

Tests of the code include examining the convergence of various properties to the continuum properties as the

	Description	$\phi(x, y, z, 0)$	$\dot{\phi}(x, y, z, 0)$
a	Ellipsoid	G	$\nu \frac{\partial G}{\partial \bar{r}} + \Omega_z (yG_{,x} - xG_{,y})$
b	Two pulses	$G_1 + G_2$	$v_1 \frac{\partial G_1}{\partial x} + v_2 \frac{\partial G_2}{\partial x}$
c	Toroid	$Ae^{-z^2/\delta^2} \times e^{-(\sqrt{\epsilon_x x^2 + \epsilon_y y^2} - R)^2/\delta^2}$	$\Omega_z (y\phi_{,x} - x\phi_{,y})$
d	Antisymmetric	$x G$	0
e	Flat Pulse	$A \left(\frac{1}{2} \tanh \frac{\hat{r}+R}{\delta} + \frac{1}{2} \right) \times \left(\frac{1}{2} \tanh \frac{-\hat{r}+R}{\delta} + \frac{1}{2} \right)$	0
f	Static (for $p = 5$)	$G + (1 + r^2/3)^{-1/2}$	0

TABLE I: List of various initial data families. For families (a)-(f) both the field $\phi(x, y, z, 0)$ and its time derivative $\dot{\phi}(x, y, z, 0)$ are shown at the initial time $t = 0$ in terms of various parameters. The terms G , G_1 , and G_2 represent unique Gaussian pulses as defined in Eq. (6). In family (b), the parameters v_1 and v_2 are the respective velocities of the two pulses, generally chosen to have a grazing collision. Family (f) represents perturbations of the static solution for the particular case of $p = 5$.

resolution is increased. To that end, the energy density associated with the scalar field is given by

$$\rho = \frac{1}{2} \left[\left(\dot{\phi} \right)^2 + (\phi_{,x})^2 + (\phi_{,y})^2 + (\phi_{,z})^2 \right] - \frac{\phi^{p+1}}{p+1}, \quad (3)$$

so that the energy contained in the grid can be computed by an integral. Similarly, the z -component of the angular momentum is [9]

$$J_z = \int d^3x M^{xy} = \int d^3x \dot{\phi} (y\phi_{,x} - x\phi_{,y}). \quad (4)$$

One example of the conservation of these quantities is presented in Fig. 1. Also in this figure is plotted the convergence factor

$$Q(t) = \frac{|\tilde{\chi}_{4h} - \tilde{\chi}_{2h}|_2}{|\tilde{\chi}_{2h} - \tilde{\chi}_h|_2} \quad (5)$$

which compares the differences in solutions as the resolution is increased. For a second order accurate scheme such as this one, the convergence factor is expected to converge to the value four. As shown in Fig. 1, the code

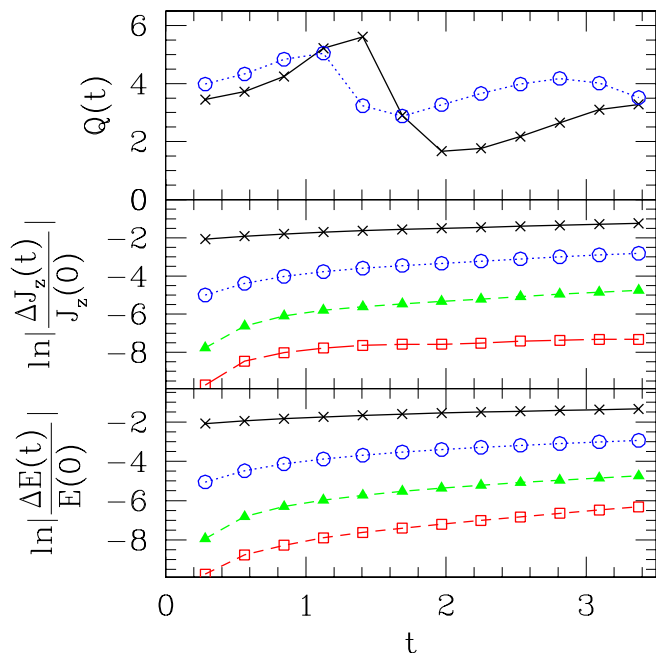


FIG. 1: Demonstration of convergence of the code for $p = 7$. The **bottom frame** displays the energy loss (relative to the initial time) $\Delta E(t) \equiv E(t) - E(0)$ for four resolutions: $(32 + 1)^3$ (solid, black crosses), $(64 + 1)^3$ (dot, blue circles), $(128 + 1)^3$ (short dash, green triangles), and $(256 + 1)^3$ (long dash, red squares). As the resolution increases, energy loss decreases. In a similar fashion the **middle frame** shows the loss of the z -component of the angular momentum as a function of time which also converges to conservation. The **top frame** shows the convergence factor $Q(t)$ as in Eq. 5 which approaches the expected value of 4 with increasing resolution. This run is a bit below the threshold for singularity formation and, as such, represents a strong field example away from the linear regime. The initial data is from family (c) (see Table I) with parameters $A = 0.14$, $\delta = 2.5$, $\epsilon_x = 2.4$, $\epsilon_y = 0.4$, $\Omega_z = 3$, and $R = 3.8$. The dimensionless ratio of the angular momentum to the energy squared is $J/E^2 = 0.013$.

demonstrates second order convergence as well as conservation of the total energy and angular momentum.

A number of families of initial data have been explored, and these are described in Table I. Initial data is created by specifying ϕ and $\dot{\phi}$ at the initial time, and is done so here with a variety of real constants. A generalized Gaussian pulse is defined as

$$G(x, y, z) = Ae^{-(\tilde{r}-R)^2/\delta^2}, \quad (6)$$

where \tilde{r} is a generalized radial coordinate

$$\tilde{r} = \sqrt{\epsilon_x(x - x_c)^2 + \epsilon_y(y - y_c)^2 + (z - z_c)^2}. \quad (7)$$

Such a pulse depends on parameters: amplitude A , shell radius R , pulse width δ , pulse center (x_c, y_c, z_c) , and

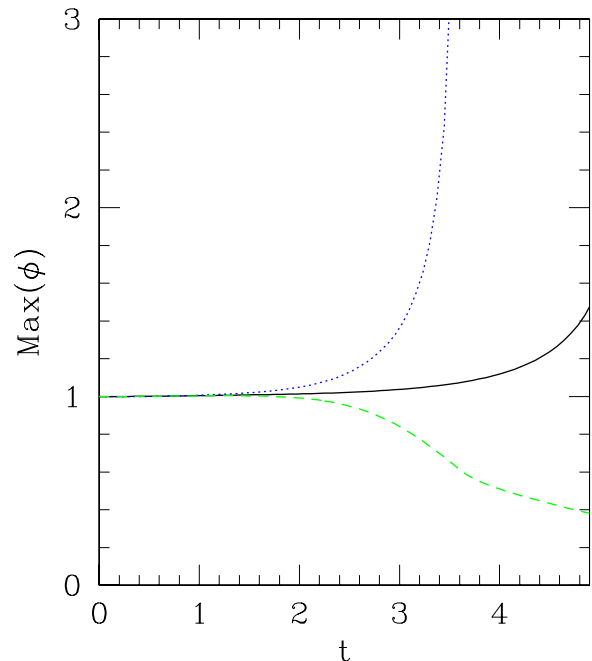


FIG. 2: Demonstration of threshold behavior of $p = 5$ static solution. The maximum value of the field is plotted for three evolutions; In solid line the results for the static solution (Family (f) in Table I) are shown. In dashed line are the maximums obtained with a perturbation with negative amplitude $A = -0.05$, $R = 6$, $\delta = 2$, $\epsilon_x = 2$, and $\epsilon_y = 0.6$. In dotted line the results with the same perturbation except with a positive amplitude $A = +0.05$ are shown. As the figure indicates, the perturbations send the solution towards either singularity formation or dispersal. Here, one can also see that at late times the unstable static solution is also driven to singularity formation because of the variety of numerical perturbations inherent in the numerical scheme such as the boundary treatment.

skewing factors ϵ_x and ϵ_y . For $\epsilon_x \neq 1 \neq \epsilon_y$ such a pulse has elliptic cross section. Family (a) represents a single pulse for which the parameter ν takes the values $\{-1, 0, +1\}$ for an approximately out-going, time-symmetric, or approximately in-going pulse, respectively. The angular momentum of the pulse about the z -axis is proportional to the parameter Ω_z as well as to $(\epsilon_x - \epsilon_y)^2$. The other families are similarly defined.

II. THRESHOLD BEHAVIOR

Solutions of Eq. (2) approach one of two end states, either dispersal or singularity formation. This situation is quite similar to the evolution of a scalar wave pulse coupled to gravity which tends toward either dispersal or black hole formation. Choptuik's study of this problem [10] found fascinating behavior at the threshold for

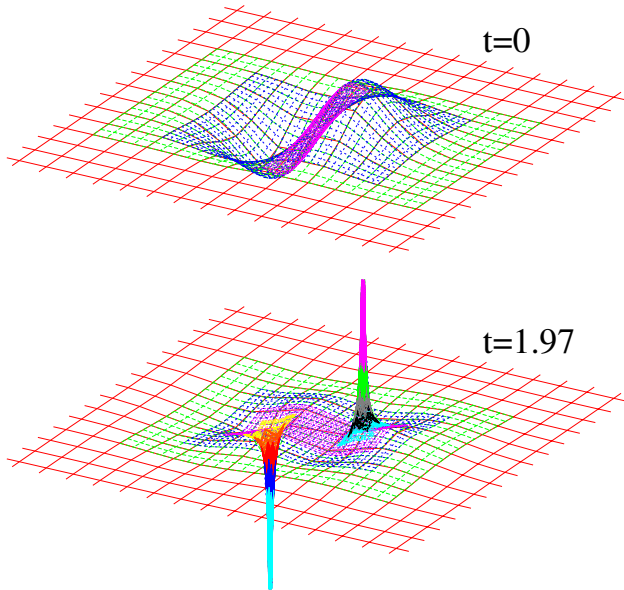


FIG. 3: Example of a slightly super-critical evolution of antisymmetric initial data (Family (d) from Table I) for $p = 5$. The first frame shows the initial field configuration $\phi(x, y, 0, 0)$ in the x - y plane and the second frame shows the two, well-resolved regions in which the field is blowing up.

black hole formation (for reviews of *black hole critical phenomena* see [11, 12]). It was largely in the spirit of Choptuik's work that the previously mentioned studies considered what happens at the threshold of singularity formation in the nonlinear sigma model [1, 2, 3, 4, 5, 6, 7].

Self-similar solutions are often found at the threshold, and indeed such is the case here. As mentioned in [8], the scaling symmetry of Eq. (1) allows for self-similar solutions of the form

$$\phi(r, t) = (T - t)^{-\alpha} U(\rho) \quad (8)$$

where

$$\rho = \frac{r}{T - t} \quad \text{and} \quad \alpha = \frac{2}{p - 1}. \quad (9)$$

Here, T is the collapse time associated with the formation of a singularity. In [8], they find discrete families of solutions, $U_n(\rho)$, for $p = 3$ and for $p = 7$, but find no nontrivial self-similar solutions for $p = 5$. Plugging Eq. (8) into Eq. (1), one arrives at an ODE that can be solved with a standard shooting method and which duplicates the results of [8].

I now consider the different cases for p in turn.

A. The case: $p = 3$

In the spherically symmetric evolutions of [8] for $p = 3$, the threshold could not be studied because evolutions

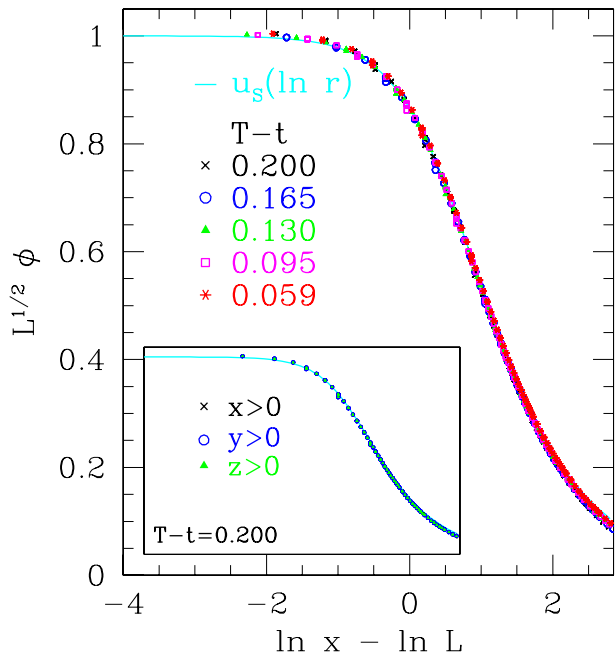


FIG. 4: Demonstration of the near critical approach to the static solution for $p = 5$. Shown are certain $x > 0$, $y = 0$, $z = 0$ slices of an evolution at five different times near the collapse time, T . Each slice $\phi(\ln x)$ is rescaled to $L^{1/2}\phi(\ln x - \ln L)$ in accordance with the rescaling symmetry of the problem. The rescaling factor $L(t)$ is chosen for each time slice in order to achieve unity at the origin. The (unrescaled) static solution $u_S(\ln r)$ is shown in solid line. The excellent agreement among these profiles suggests the solution represents a *scale evolving static solution*. The inset shows three different slices along the three positive axes all at the same time, and indicates that the central area of the solution is spherically symmetric. The initial data come from family (a) of Table I with $R = 3$, $\delta = 2$, $x_c = 0 = y_c = z_c$, $\epsilon_x = 2$, $\epsilon_y = 0.7$, $\nu = 0$, and $\Omega_z = 0.1$, and the evolution entails 11 levels of 2:1 refinement with a 33^3 coarse grid.

that looked to be dispersing would eventually demonstrate growth near the origin, and hence the threshold of singularity formation could not be studied. Similar problems are encountered here even without the assumption of spherical symmetry.

B. The case: $p = 5$

In spherical symmetry [8], no nontrivial self-similar solution exists for $p = 5$, and evolutions near the threshold approach the known static solution

$$u_S(r) = \frac{1}{\sqrt{1 + r^2/3}}. \quad (10)$$

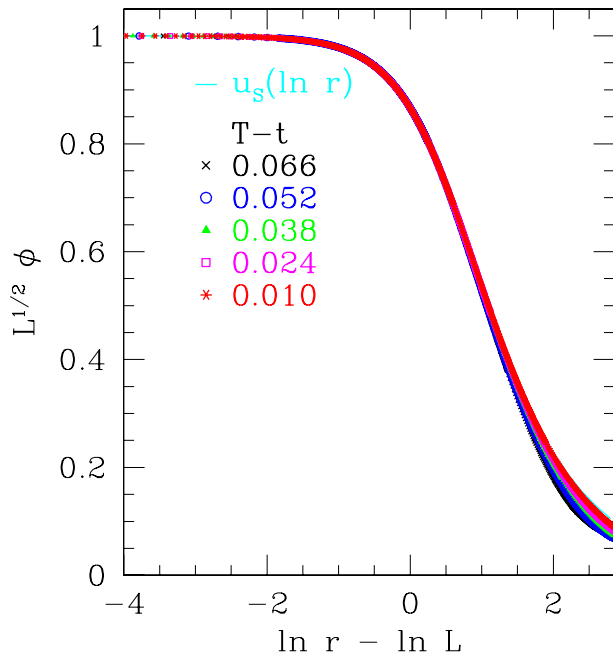


FIG. 5: Near-critical solution from the explicitly spherically symmetric code for $p = 5$ with initial data family (12) and (13) and $R = 0.1$, $\delta = 0.3$, and $A^* \approx 5.539$. Similar to Fig. 4, the solution at times near the collapse time is shown rescaled. Its agreement with the (unrescaled) static solution (shown in solid line) suggests a scale evolving static solution.

Retaining the notation of [8], we have a family of static solutions, u_S^L , generated by rescalings of (10)

$$u_S^L(r) = L^{-1/2} u_S(r/L). \quad (11)$$

In three dimensions without the assumption of spherical symmetry, the static solution remains at the threshold of singularity formation. In Fig. 2, the maximum value of the scalar field within the computed domain is plotted versus time. For the static solution, this value remains essentially constant until late times when inherent numerical perturbations drive it to form a singularity. Also plotted are the results of initial data consisting of the static solution along with a small Gaussian pulse added explicitly to perturb the solution. For positive amplitude of the Gaussian pulse, the solution is driven to singularity formation whereas for negative amplitude the solution disperses. These results suggest that the static solution remains on threshold even without the assumption of spherical symmetry.

However, for other families of initial data near the threshold, the evolution does not appear static. Instead, the collapsing region appears roughly self-similar in its collapse about some central point. Consider for example a family of initial data which is antisymmetric across the y - z plane, Family (d) from Table I. One such example is

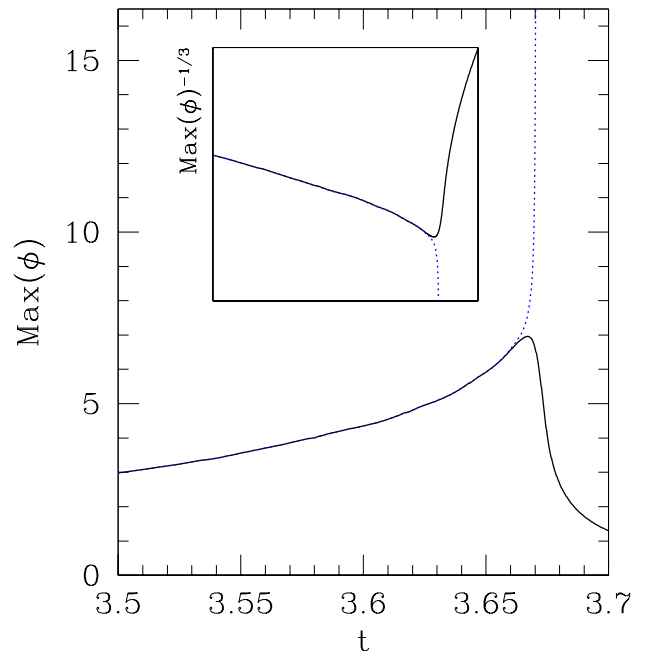


FIG. 6: Results from two near critical evolutions for $p = 7$ with initial data family (e). The maximum of the field configuration ϕ is plotted versus time for a slightly subcritical evolution (solid) and for a slightly super-critical evolution (dotted). The collapse time T is estimated by determining the lifetime of the supercritical evolution closest to criticality, in this case $T \approx 3.67$. The inset shows the same information with the expected scaling of ϕ .

shown in Fig. 3. The first frame in the figure shows the initial configuration for ϕ and the second frame shows the solution near the collapse time. Two regions of collapse form with both regions spherically symmetric about their respective centers.

That the collapse appears self similar when no such solution is admitted also occurs in the case of blowup with a Yang-Mills field [13, 14]. There, the dynamics were identified with a *scale evolving static solution*, and such an identification appears to be the case here.

Evidence that the near critical solution represents the static solution with a scale factor dependent on time, $L(t)$, is presented for a particular case in Fig. 4. Shown in the figure is the evolution at different times near the collapse time rescaled according to Eq. (11) by choosing $L(t)$ such that the rescaled quantity $\sqrt{L}\phi(r=0)$ is unity. The (unrescaled) static solution, u_S , is also shown and the excellent agreement among the profiles is strong evidence that indeed the evolution is proceeding along the scale evolving static solution.

The inset of Fig. 4 shows three different spatial slices of the data for a particular time. They agree quite well, providing good evidence that the solution is spherically

C. The case: $p = 7$

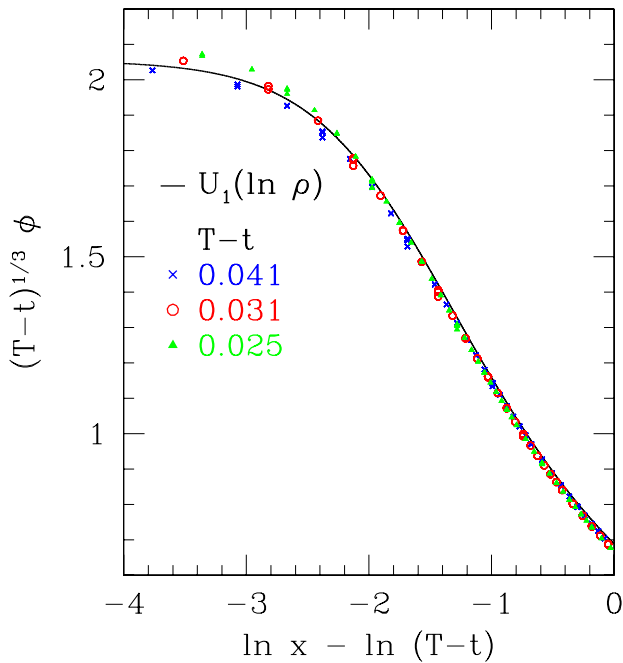


FIG. 7: Demonstration of self-similarity of a near-critical solution for $p = 7$. This is similar to Fig. 4 and indeed has the same initial data family (with different critical amplitude A^*). That the solutions at different times t coincide indicates self-similarity. Also shown is the explicitly self-similar solution $U_1(\rho)$ found by solving an ODE. The collapse time T is determined by the average of the values required for each time slice to achieve agreement with U_1 for $\rho = 0$.

symmetric.

One can observe similar behavior in spherical symmetry by modifying the code from [3]. For many families of initial data, near threshold solutions approach the static solution in the conventional way. However, in Fig. 5 a near critical solution is shown obtained by tuning the initial data family

$$\phi(r, 0) = \frac{A}{2} \left[\tanh \left(\frac{R-r}{\delta^2} \right) + 1 \right] \quad (12)$$

with the initial time derivative set consistent with Eq. (8)

$$\dot{\phi}(r, 0) = \frac{\phi(r, 0)}{2} + r \frac{d\phi(r, 0)}{dr}. \quad (13)$$

For this family, near threshold solutions also appear to approach a scale evolving static solution.

In [8] for the $p = 7$ case, they find in the critical limit an approach to the $U_1(\rho)$ self-similar solution. Here, without the assumption of spherical symmetry, similar threshold behavior is observed (see Fig. 6). Such a near critical solution is shown in Fig. 7. The solution appears both self-similar and spherically symmetric. The inset of Fig. 7 compares the obtained solution to the ODE solution, $U_1(\rho)$, and they appear quite similar suggesting that it remains the critical solution even without the assumption of spherical symmetry.

III. CONCLUSIONS

The semilinear wave equation represents perhaps the simplest nonlinear generalization of the linear wave equation, and yet it displays interesting threshold behavior. In particular, this work has extended the results of [8] obtained in spherical symmetry to the full 3D case.

For the $p = 3$ case, the threshold could not be studied because of its late time growth which was also observed in spherical symmetry.

For the $p = 5$ case, a critical solution is observed which appears roughly self similar despite the fact that no such solution is admitted. Instead, the solutions suggest an approach to the static solution with an evolving scale. This same behavior is also observed in a code which explicitly assumes spherical symmetry.

For the $p = 7$ case, a critical solution is found which resembles that found in the spherically symmetric case.

Acknowledgments

This research was supported in part by NSF cooperative agreement ACI-9619020 through computing resources provided by the National Partnership for Advanced Computational Infrastructure at the University of Michigan Center for Advanced Computing and by the National Computational Science Alliance under PHY030008N. This research was also supported in part by NSF grants PHY0325224 and PHY0139980 and by Long Island University.

[1] J. Isenberg and S. Liebling, *J. Math. Phys.* **43**, 678 (2002).

[2] P. Bizoń, T. Chmaj, and Z. Tabor, *Nonlinearity* **14**, 1041 (2001).

- [3] S. L. Liebling, E. W. Hirschmann, and J. Isenberg, *J. Math. Phys.* **41**, 5691 (2000), math-ph/9911020.
- [4] P. Bizoń, T. Chmaj, and Z. Tabor, *Nonlinearity* **13**, 1411 (2000).
- [5] S. L. Liebling, *Pramana* **55**, 497 (2000), gr-qc/0006005.
- [6] S. L. Liebling, *Phys. Rev.* **D66**, 041703(R) (2002), gr-qc/0202093.
- [7] S. L. Liebling, *Class. Quant. Grav.* **21**, 3995 (2004), gr-qc/0403076.
- [8] P. Bizoń, T. Chmaj, and Z. Tabor (2003), math-ph/0311019.
- [9] L. H. Ryder, *Quantum Field Theory* (Cambridge University Press, 1996).
- [10] M. W. Choptuik, *Phys. Rev. Lett.* **70**, 9 (1993).
- [11] M. W. Choptuik (1997), gr-qc/9803075.
- [12] C. Gundlach, *Adv. Theor. Math. Phys.* **2**, 1 (1998), gr-qc/9712084.
- [13] P. Bizoń and Z. Tabor, *Phys. Rev.* **D64**, 121701(R) (2001), math-ph/0105016.
- [14] P. Bizoń, *Acta Phys. Polon.* **B33**, 1893 (2002), math-ph/0206004.